Application of Meshless Method in Numerical Simulation of Solitary Waves for the Generalized Regularized Long Wave Equation

Huiling Chen, Rahmatjan Imin, Azhar Halik

Abstract—**This study proposes an enhanced meshless Smoothed Particle Hydrodynamics (SPH) method for solving the 1D Generalized Regularized Long Wave Equation (GRLW) with nonlinear dispersion properties. The method innovatively combines the Crank-Nicolson temporal discretization scheme with Kernel Derivative Free-SPH (KDF-SPH) spatial approximation, establishing an unconditionally stable semi-implicit conservative scheme. To further validate the performance of the method, the reliability of the KDF-SPH method is systematically verified through simulations of single solitary wave propagation, interaction between two solitary waves and waveform evolution processes. Evaluation based on three conservation invariants and error norms shows that the proposed method not only effectively preserves the conservation properties of the equation but also exhibits superior computational accuracy. Comparative analysis with existing numerical methods clearly reveals that the method achieves higher computational precision and better simulation performance, conclusively verifying its accuracy and effectiveness in solving the GRLW equation.**

Index Terms—**KDF-SPH method; GRLW equation; the stability analysis; numerical simulation**

I. Introduction

The continuous advancement of disciplines including fluid mechanics and engineering mechanics, together with emerging technologies and associated theoretical developments, has led to the derivation of a class of nonlinear Partial Differential Equations (PDEs) characterizing fluid phenomena and engineering mathematical models in these domains. For instance, the Advection-Diffusion-Reaction Equation (ADRE) has been widely used in many fields of science and engineering related to fluid dynamics and molecular diffusion [1]. The Korteweg-de Vries Equation (KdV) is widely applied across diverse domains, including fluid dynamics, plasma physics, optical fiber communication and the mathematical physics, etc. For practical problems, obtaining exact analytical solutions for these equations is quite difficult. Therefore, the study of numerical methods for nonlinear PDEs holds both significant academic value and substantial practical importance in addressing real-world applications.

Regularized long wave (RLW) equation

$$u_t + \nabla u + \alpha u \nabla u - \beta \Delta u_t = 0, \tag{1}$$

where both α and β are positive constants. $u_t + \nabla u$ is a linear wave propagation term, indicating that the wave propagates at a constant velocity to the right. The term $u\nabla u$ is a nonlinear term, reflecting the effect of wave amplitude on propagation velocity. The term Δu_t serves dual roles as a dispersion term and a regularization term. By suppressing high-frequency short-wave oscillations, it enhances the model's physical validity in long-wave regimes. In nonlinear wave equations, this dual functionality balances nonlinear effects to permit stable solitary wave formation.

RLW equation was originally proposed by D.H. Peregrine [2] in 1966. Due to its effectiveness in modeling physical processes including soliton propagation, electromagnetic waves, and acoustic waves, this equation has become a paradigm in several research fields. The wave motion RLW equation describes coincides with the approximate solutions of the KdV, and it also effectively simulates nearly all applications of the KdV, which has attracted significant research attention. The RLW equation is especially effective in modeling wave-dominated systems, as it can capture the nonlinear characteristics of wave propagation and accounts for dispersive effects. Therefore, the research of the RLW equation not only enriches our understanding of nonlinear dynamics but also offers valuable solutions to the wave-related engineering challenges. In fact, the GRLW equation is a generalization of RLW equation. GRLW introduces a more general nonlinear term based on the RLW equation, and its expression is as follows

$$u_t + \nabla u + \alpha u^p \nabla u - \beta \Delta u_t = 0, \tag{2}$$

where p is a positive integer. When $p = 1$, the GRLW equation (2) corresponds to the RLW equation, i.e., equation (1). When $p = 2$, the GRLW equation (2) corresponds to modified regularized long wave (MRLW) equation.

The GRLW equation's nonlinear term makes analytical solutions generally intractable. Therefore, many researchers have conducted extensive studies on numerical solutions of this equation under initial and boundary conditions. For the

Manuscript received March 15, 2025; revised May 25, 2025.

This work was supported by National Natural Science Foundation of China, Grant No:12462028.

Huiling Chen is a postgraduate student of the College of Mathematical and Systems Science in Xinjiang University, Urumqi 830017, China (e-mail: 1802748003@qq.com).

Rahmatjan Imin is an associate professor of the College of Mathematical and Systems Science in Xinjiang University, Urumqi 830017, China (e-mail: rahmatjanim@xju.edu.cn).

Azhar Halik is an associate professor of the College of Mathematical and Systems Science in Xinjiang University, Urumqi 830017, China (e-mail: azhar@xju.edu.cn).

RLW, Kutluay et al. [3] proposed a linearized implicit finite difference scheme for numerical solution of the 1D RLW equation. Sun et al. [4] discretized the spatial and temporal domains using the cosine differential quadrature method and finite difference method respectively, and constructed a numerical scheme for solving the RLW equation through Crank-Nicolson linearization technique. Görgülü et al. [5] discretized both the spatial and temporal derivatives of the RLW equation using the exponential B-spline Galerkin method and Crank-Nicolson scheme respectively, with numerical examples validating the method's accuracy. Yang et al. [6] proposed a higher-order compact finite difference scheme for the 1D RLW equation, and verified its accuracy and reliability through numerical experiments. For numerical solution of the MRLW equation, Raslan [7] proposed a novel algorithm in 2009 employing the collocation method. Cai [8] constructed a ten-point multi-symplectic explicit scheme for the MRLW equation, in which the nonlinear term is absent at the third temporal level. Gao [9] proposed a mixed Galerkin finite element method for numerical investigation of the MRLW equation. Jena et al. [10] proposed a numerical method for the MRLW combining Butcher's fifth-order Runge-Kutta scheme with quartic B-spline functions. For the study of GRLW equation, Xu et al. [11] developed a two-level nonlinear conservative finite difference scheme for the numerical solution of GRLW Equation. Hammad et al. [12] proposed a Chebyshev-Chebyshev spectral collocation method based on Kronecker and Hadamard products for solving the GRLW equation. Through theoretical research, Zheng et al. [13] obtained bifurcation solutions and exact traveling wave solutions for the GRLW. Kumari et al. [14] developed a numerical scheme for solving the GRLW equation based on orthogonal collocation in the finite element method and septic Hermite collocation.

The SPH method is a novel meshless method. It employs discrete particles to simulate fluid flows, with each particle carrying fundamental physical properties such as density, viscosity, mass, velocity, and temperature [15]. SPH was originally proposed by Lucy [16] in 1977, primarily for solving astrophysical problems in three-dimensional unbounded space. Due to its adaptive nature and the meshless characteristic enabling accurate simulation of complex geometric boundaries, the SPH method has been widely adopted in free-surface fluid dynamics research. However, due to the discontinuous nature of particles, SPH exhibits relatively low computational accuracy. To overcome this drawback, most researchers have conducted extensive studies and proposed enhanced variants, including CSPM [17], MSPH [18] and the KDF-SPH method, all of which significantly improve numerical precision.

Through a comprehensive literature review, it is found that existing studies have not yet applied KDF-SPH to solve GRLW equation. Consequently, this study implements KDF-SPH for the first time to simulate GRLW equation numerically. The subsequent sections of this paper are organized as follows: In section 2, we introduce various types of the GRLW equation. Section 3 presents the theoretical foundations of both SPH and KDF-SPH. In Section 4, the GRLW equation is discretized to obtain a semi-implicit discrete scheme. Section 5 conducts a stability analysis of the discrete formulation derived in Section 4. In Section 6, we employ the KDF-SPH method to numerically simulate the GRLW equation and analyzes the obtained numerical results. Finally, we draw some conclusions and propose future perspectives in Section 7.

II. GRLW EQUATION

The GRLW equation can describe more complex nonlinear wave phenomena. For example, under certain conditions, the GRLW equation can admit soliton solutions, which are waves that maintain constant shape and speed during propagation. The GRLW equation can also be used to study the collisions and interactions between multiple solitons. By adjusting the nonlinear and dispersive terms, the GRLW equation can model wave propagation behaviors in different physical systems. This paper mainly studies the following three forms of the GRLW equation.

A. RLW equation

When $p=1$ in equation (2), we consider RLW equation defined on the spatial domain $\Omega=[x_L,x_R]$ with Dirichlet boundary conditions:

$$\begin{cases} u_t+u_x+\alpha uu_x-\beta u_{xxt}=0,(x,t)\in\Omega\times[0,T], \\ u(x,0)=U(x,0),x\in\Omega\times\{t=0\}, \\ u(x_L,t)=U(x_L,t),u(x_R,t)=U(x_R,t),t=[0,T]. \end{cases} \tag{3}$$

According to reference [19], the RLW equation has only three conservation properties, namely the conservation of mass(I_1),momentum(I_2) and energy(I_3) defined as follows

$$\begin{aligned} I_1&=\int_a^b u dx, \\ I_2&=\int_a^b [u^2+\beta(u_x)^2]dx, \\ I_3&=\int_a^b [u^3+3u^2]dx. \end{aligned} \tag{4}$$

The RLW equation is capable of modeling a wide range of physical phenomena characterized by weakly nonlinear and dispersive wave propagation. Typical applications include: nonlinear transverse wave dynamics in shallow water environments, dispersive longitudinal wave propagation through elastic solid rods, and other related phenomena.

B. MRLW equation

When $p=2$ in equation (2), we consider MRLW equation defined on the spatial domain $\Omega=[x_L,x_R]$ with Dirichlet boundary conditions:

$$\begin{cases} u_t+u_x+6u^2u_x-u_{xxt}=0,(x,t)\in\Omega\times[0,T] \\ u(x,0)=U(x,0),x\in\Omega\times\{t=0\}, \\ u(x,t)=U(x,t),(x,t)\in\partial\Omega\times[0,T]. \end{cases} \tag{5}$$

According to reference [20], the MRLW equation also has three conservation laws, namely the conservation of mass(I_1), momentum(I_2) and energy(I_3) defined as follows

$$I_1 = \int_a^b u dx,$$
$$I_2 = \int_a^b [u^2 + \beta (u_x)^2] dx, \quad (6)$$
$$I_3 = \int_a^b [u^4 - \beta (u_x)^2] dx.$$

The MRLW equation can effectively characterize the evolution of weakly nonlinear dispersive waves, and resolve the short-wavelength singularities inherent in conventional long-wave equations. And this equation plays a significant role in simulating long-wave disturbances and modeling dispersive media with small amplitudes [21].

C. GRLW equation

When $p \geq 3$ in equation (2), we consider the GRLW equation subject to the following initial-boundary value conditions:

$$\begin{cases} u_t + u_x + \alpha u^p u_x - \beta u_{xxt} = 0, (x,t) \in \Omega \times [0,T], \\ u(x,0) = U(x,0), (x,t) \in \Omega \times \{t = 0\}, \\ u(x,t) = U(x,t), (x,t) \in \partial\Omega \times [0,T]. \end{cases} \quad (7)$$

In summary, the GRLW equation exhibits enhanced universality and broader applicability, enabling the modeling of a wider spectrum of nonlinear wave phenomena.

III. SPH METHOD

A. The traditional SPH method

The process of using SPH to solve partial differential equations can be briefly outlined as follows [22]: First, the computational domain is discretized into a collection of particles with physical properties to simulate a continuous medium. Then, the governing equation is transformed into ordinary differential equation. Finally, the numerical solution of the governing equation is obtained through weighted integration using kernel function interpolation. SPH's core is its interpolation approximation, primarily consisting of kernel approximation and particle approximation.

Kernel approximation

For 1D problems, any continuous and smooth function $\varphi(x)$ can be approximated by the following expression

$$\varphi(x) \approx \int_\Omega \varphi(x') \delta(x - x') dx', \quad (8)$$

where Ω is the integration domain, and $\delta(x - x')$ is the Dirac function.

The Dirac function in equation (8) can be replaced by a kernel function, and the kernel approximation expression of $\varphi(x)$ can be obtained. To distinguish it, we use $\langle \varphi(x) \rangle$ to represent it,

$$\langle \varphi(x) \rangle = \int_\Omega \varphi(x') W(x - x', h) dx', \quad (9)$$

where Ω is the influence region of the kernel function, $W(x - x', h)$ represents the smoothing kernel function, and h is the smoothing length.

To obtain the nth-order derivative of $\varphi(x)$, take the nth-order derivative of equation (8) with respect to x,

$$\left\langle \frac{d^n \varphi(x)}{dx^n} \right\rangle = \int_\Omega \varphi(x') \frac{d^n}{dx^n} W(x - x', h) dx'. \quad (10)$$

Particle approximation

The region Ω is discretized into a collection of particles with physical properties. For the j-th particle in the domain, its volume is V_j and its density is ρ_j. Using V_j to represent the volume of the infinitesimal element dx', the kernel approximation expressions (9) and (10) for the continuous and smooth function $\varphi(x)$ can be translated as

$$\langle \varphi(x) \rangle = \sum_{j=1}^{N} \frac{m_j}{\rho_j} \varphi(x_j) W(x - x_j, h), \quad (11)$$
$$\left\langle \frac{d^n \varphi(x)}{dx^n} \right\rangle = \sum_{j=1}^{N} \frac{m_j}{\rho_j} \varphi(x_j) \frac{d^n}{dx^n} W(x - x_j, h), \quad (12)$$

where N represents the total number of particles within the support domain of the kernel function, and $x \neq x_j$.

B. KDF-SPH Method

To perform a Taylor expansion of the smooth continuous function $\varphi(x')$ at the point x [23],

$$\varphi(x') = \sum_{n=0}^{\infty} \frac{\varphi^{(n)}(x)}{n!} (x' - x)^n = \sum_{n=0}^{\infty} \frac{h^n}{n!} \varphi^{(n)}(x) \left(\frac{x' - x}{h}\right)^n, \quad (13)$$

where $\varphi^{(n)}(x)$ denotes the n-th derivative of the function φ at the point x.

Multiply both sides of equation (13) by $\frac{x' - x}{h} W(x - x', h)$, and perform the integration within the influence domain of the kernel function, we can obtain the expression

$$\left\langle \frac{x' - x}{h} \varphi(x) \right\rangle = \sum_{n=0}^{2} \frac{h^n}{n!} M_{n+1} \varphi^{(n)}(x) + o(h^3), \quad (14)$$

where $M_{n+1} = \int_\Omega \left(\frac{x' - x}{h}\right)^{n+1} W(x - x', h) dx'$ for $n = 0, 1, 2, \ldots$, are the moments of the one-dimensional kernel function, and they are constants independent of the kernel function.

Based on the properties of the kernel function, it is known that $M_1 = M_3 = 0$. Therefore, the first-order derivative of function φ at point x can be derived from equation (14) as follows

$$\varphi'(x) = \frac{\left\langle \frac{x' - x}{h} \varphi(x') \right\rangle}{h M_2} + o(h^2). \quad (15)$$

Similarly, multiplying both sides of equation (13) by

$\left(\frac{x'-x}{h}\right)^2 W(x-x',h)$ and integrating over the kernel support domain Ω yields

$$\left\langle \left(\frac{x'-x}{h}\right)^2 \varphi(x) \right\rangle = \sum_{n=0}^{3} \frac{h^n}{n!} M_{n+2} \varphi^{(n)}(x) + o(h^4), \quad (16)$$

where M_{n+2} are also moments of the one-dimensional kernel function, for $n = 0,1,2,\ldots$, defined as above.

Using the properties of the kernel function: $M_3 = M_5 = 0$, the second-order derivative of $\varphi(x)$ at point x can be obtained from equation (16),

$$\varphi''(x) = \frac{\left\langle \left(\frac{x'-x}{h}\right)^2 \varphi(x') \right\rangle - M_2 \varphi(x)}{\frac{h^2}{2} M_4} + o(h^2). \quad (17)$$

IV. The Discretization Of The GRLW Equation

Consider the following equation

$$u_t + u_x + \alpha u^p u_x - \beta u_{xxt} = 0. \quad (18)$$

First, applying the Crank-Nicolson scheme [24] to discretize equation (18) yields the rearranged expression

$$\begin{aligned} &u^{n+1} + \frac{dt}{2}\left[u_x^{n+1} + \alpha (u^p)^n u_x^{n+1}\right] - \beta u_{xx}^{n+1} = \\ &u^n - \frac{dt}{2}\left[u_x^n + \alpha (u^p)^n u_x^n\right] - \beta u_{xx}^n. \end{aligned} \quad (19)$$

Then, for the point x_i in the discretized domain, applying KDF-SPH described in Section 3 to equation (19) yields

$$\begin{aligned} &u_i^{n+1} + \frac{dt}{2}\Bigg[\frac{\sum_{j=1}^{N} \frac{m_j}{\rho_j} \frac{x_j - x_i}{h} u_j^{n+1} W_{ij}}{hM_2} \\ &+ \alpha \left(u_i^p\right)^n \frac{\sum_{j=1}^{N} \frac{m_j}{\rho_j} \frac{x_j - x_i}{h} u_j^{n+1} W_{ij}}{hM_2^x}\Bigg] - \\ &\beta \frac{2\left[\sum_{j=1}^{N} \frac{m_j}{\rho_j} \left(\frac{x_j - x_i}{h}\right)^2 u_j^{n+1} W_{ij} - M_2 u_i^{n+1}\right]}{h^2 M_4} = u_i^n - \\ &\frac{dt}{2}\Bigg[\frac{\sum_{j=1}^{N} \frac{m_j}{\rho_j} \frac{x_j - x_i}{h} u_j^n W_{ij}}{hM_2} + \alpha (u_i^p)^n \frac{\sum_{j=1}^{N} \frac{m_j}{\rho_j} \frac{x_j - x_i}{h} u_j^n W_{ij}}{hM_2^x} \\ &- \beta \frac{2\left[\sum_{j=1}^{N} \frac{m_j}{\rho_j} \left(\frac{x_j - x_i}{h}\right)^2 u_j^n W_{ij} - M_2 u_i^n\right]}{h^2 M_4} \end{aligned} \quad (20)$$

where i and j denote the i-th particle and the j-th particle in the discretized domain, respectively.

Finally, assembling the equation (20) corresponding to each discrete point in the domain Ω forms a matrix, we can obtain

$$\left[E + \frac{dt}{2}[A + \alpha BA] - \beta C\right] U^{n+1} = \left[E - \frac{dt}{2}[A + \alpha BA] - \beta C\right] U^n, \quad (21)$$

where E is an identity matrix,

$$A = \begin{bmatrix} \frac{\frac{m_1}{\rho_1}\frac{x_1 - x_1}{h} W_{11}}{hM_2} & \cdots & \frac{\frac{m_N}{\rho_N}\frac{x_N - x_1}{h} W_{1N}}{hM_2} \\ \frac{\frac{m_1}{\rho_1}\frac{x_1 - x_2}{h} W_{21}}{hM_2} & \cdots & \frac{\frac{m_N}{\rho_N}\frac{x_N - x_2}{h} W_{2N}}{hM_2} \\ \vdots & \vdots & \vdots \\ \frac{\frac{m_1}{\rho_1}\frac{x_1 - x_N}{h} W_{N1}}{hM_2} & \cdots & \frac{\frac{m_N}{\rho_N}\frac{x_N - x_N}{h} W_{NN}}{hM_2} \end{bmatrix},$$

$$B = \begin{bmatrix} \left(u_1^p\right)^n & 0 & \cdots & 0 \\ 0 & \left(u_2^p\right)^n & \cdots & 0 \\ \vdots & \vdots & \ddots & \vdots \\ 0 & 0 & \cdots & \left(u_N^p\right)^n \end{bmatrix},$$

$$C = \begin{bmatrix} C_1 \\ C_2 \\ \vdots \\ C_N \end{bmatrix}, \text{ where } C_i = \begin{cases} \frac{2\left[0 - \sum_{j=1}^{N} \frac{m_j}{\rho_j} \left(\frac{x_j - x_i}{h}\right)^2 W_{ij}\right]}{h^2 M_4}, & i = j \\ \frac{2\frac{m_j}{\rho_j} \left(\frac{x_j - x_i}{h}\right)^2 W_{ij}}{h^2 M_4}, & i \neq j \end{cases},$$

$$U^{n+1} = \begin{bmatrix} u_1^{n+1} & u_2^{n+1} & \cdots & u_N^{n+1} \end{bmatrix}^T, U^n = \begin{bmatrix} u_1^n & u_2^n & \cdots & u_N^n \end{bmatrix}^T.$$

V. Stability Analysis

This section discusses the stability of matrix (21).

Assuming that u^p in the term $u^p u_x$ is a local constant, and letting the exact solution of the GRLW equation at the n-th time level be U^n and the numerical solution be u^n, the error can be expressed as

$$e^n = U^n - u^n, \quad (22)$$

Therefore, the error in equation (21) can be expressed as

$$\left[D + \frac{dt}{2} F\right] e^{n+1} = \left[D - \frac{dt}{2} F\right] e^n, \quad (23)$$

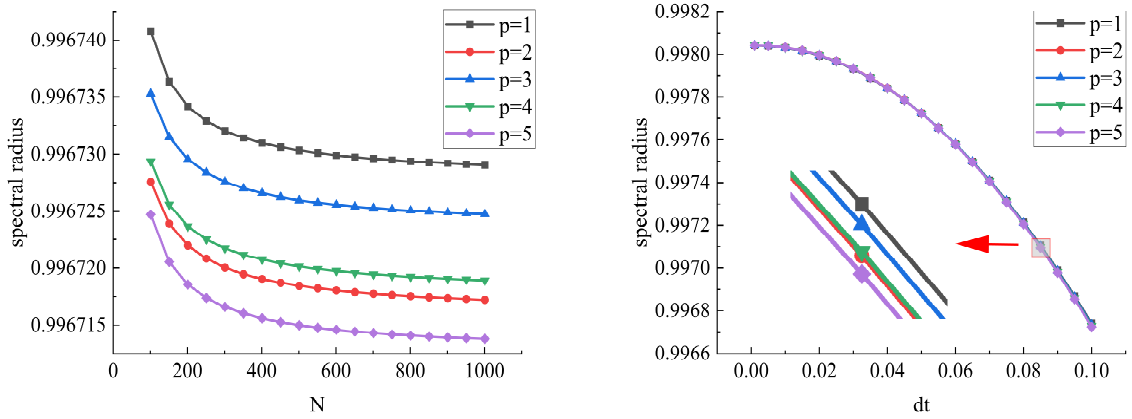

(a) $\rho(Z)$ under various particle numbers N (b) $\rho(Z)$ under various particle numbers dt

Fig. 1. Spectral radius with respect to the number of particles and time interval

where $D=[E-\beta C]$, $F=[A+\alpha BA]$.

Let $X=[D+\frac{dt}{2}F]$ and $Y=[D-\frac{dt}{2}F]$, the error equation can be transformed into

$$e^{n+1}=X^{-1}Ye^{n}=Ze^{n}. \tag{24}$$

To analyze the stability of this matrix (21), we need to consider the properties of matrix Z. Specifically, we focus on the eigenvalues of this matrix. If the modulus of all eigenvalues of matrix Z is less than or equal to 1, in other words, if $\rho(Z)$ is less than or equal to 1, then matrix (21) is considered to be stable [25].

Analysis of the matrix Z reveals that its spectral radius $\rho(Z)$ depends on the number of particles in the discretized domain and the time step. Figure 1 illustrates the influence of N and dt on the value of $\rho(Z)$ under different values of p. As shown in the figure 1, $\rho(Z)$ is always less than 1. Therefore, the above analysis confirms that the matrix (21) is stable, which implies that the scheme (19) is unconditionally stable.

VI. Numerical Experiment And Results

In this section, to assess the effectiveness of KDF-SPH, we conduct systematic numerical experiments to test the accuracy of KDF-SPH. The numerical experiments include the propagation of solitary waves and the evolution of wave profiles. The error analysis of the experimental results uses the L_2 [19] and L_∞ norm errors, defined as follows

$$L_2=\sqrt{dx\sum_{j=0}^{N}\left|U_j-u_j\right|^2}, \tag{25}$$

$$L_\infty=\max_j\left|U_j-u_j\right|, \tag{26}$$

where U_j and u_j denote the exact and numerical solutions at x_j, respectively, and dx denotes the distance between two discrete points within the computational region Ω.

SPH and KDF-SPH use the cubic B-spline kernel function [26], defined as follows

$$W(x-x',h)=\gamma_d\times\begin{cases}\frac{2}{3}-R^2+\frac{1}{2}R^3, & 0\le R<1;\\ \frac{1}{6}(2-R)^3, & 1\le R<2;\\ 0, & R\ge 2,\end{cases} \tag{27}$$

where d represents the dimension of the function. The coefficient γ_d takes values of $\frac{1}{h}$ for 1D space and $\frac{15}{7\pi h^2}$ for 2D space. And $R=\frac{r}{h}=\frac{|x-x'|}{h}$, r represents the distance between the points x and x'.

Moreover, to verify the conservation properties of the GRLW equation, this study calculates the values of I_1, I_2 and I_3. The three conservation laws of the RLW equation are given by

$$\begin{aligned} I_1&\cong dx\sum_{i=1}^{N}u_i^n,\\ I_2&\cong dx\sum_{i=1}^{N}\left[(u_i^n)^2+\beta((u_x)_i^n)^2\right],\\ I_3&\cong dx\sum_{i=1}^{N}\left[(u_i^n)^3+3(u_i^n)^2\right]. \end{aligned} \tag{28}$$

Similarly, the three conservation laws I_1, I_2 and I_3 of the MRLW equation are given by

$$\begin{aligned} I_1&\cong dx\sum_{i=1}^{N}u_i^n,\\ I_2&\cong dx\sum_{i=1}^{N}\left[(u_i^n)^2+\beta((u_x)_i^n)^2\right],\\ I_3&\cong dx\sum_{i=1}^{N}\left[(u_i^n)^4-\beta((u_x)_i^n)^2\right]. \end{aligned} \tag{29}$$

A. RLW Equation

In this section, we conduct an in-depth investigation into the dynamical behaviors of both single solitary wave motion and two solitary waves motion of the RLW equation.

Single solitary wave motion

Considering the RLW equation (3), its exact solution [27] is given by

$$U(x,t)=3c\,\mathrm{sech}^2\left[k(x-vt-x_0)\right],(x,t)\in R\times[0,T], \quad (30)$$

where v is the solitary wave velocity, $v=1+\alpha c$, and k is the wave width, $k=\frac{1}{2}\sqrt{\frac{\alpha c}{\beta v}}$. $3c$ represents the amplitude and x_0 represents the initial position of the wave.

For this problem, Zaki [28] provides the analytical values of I_1, I_2 and I_3 as follows

$$I_1=\frac{6c}{k}, I_2=\frac{12c^2}{k}+\frac{48kc^2\beta}{5}, I_3=\frac{36c^2(4c+5)}{5k}. \quad (31)$$

Case 1 We take $\alpha=1,\ \beta=1,\ x_0=0,$ and choose the spatial domain $\Omega=[-40,60]$. Firstly, the analytical values of three invariants are computed for the RLW equation. When $c=0.03$, the invariants are $I_1=2.1094,\ I_2=0.1273$ and $I_3=0.3888$. When $c=0.1$, the three invariants are $I_1=3.9800,\ I_2=0.8105$ and $I_3=2.5790$. The three values I_1, I_2, and I_3 for a single solitary wave of the RLW equation with $dx=0.5$, $dt=0.1$ and $c=0.03$, $c=0.1$ at different time are listed in TABLE I. The results in the table demonstrate agreement with their corresponding analytical values and indicate that KDF-SPH conserves mass, energy, and momentum. TABLE II displays the computed L_2 norm error and L_∞ norm error under two different amplitude conditions $c=0.03$ and $c=0.1$. The table indicates that as the value of c decreases, the two error norms gradually decrease, and the resulting error norms are also relatively small. Figure 2 presents the absolute error obtained using KDF-SPH and SPH. This space–time graph indicates that the results obtained by KDF-SPH are closer to the analytical solution and produce smaller absolute errors. Figure 3 demonstrates the matching effect between the exact solution and the numerical solution at different time for $N=101$, $dt=0.1$ and $c=0.03$. This figure shows that the numerical solution obtained by KDF-SPH exhibit excellent agreement with the exact solution. Moreover, the solitary wave propagates to the right over time while maintaining nearly constant amplitude. The stable amplitude of solitary waves in shallow water enables optimized breakwater design through prediction of persistent impact forces, enhancing structural durability.

TABLE I

VALUES OF THE CONSERVED QUANTITIES WITH $dx=0.5,\ dt=0.1$ AT DIFFERENT MOMENTS

Time	$c=0.03$			$c=0.1$		
	I_1	I_2	I_3	I_1	I_2	I_3
t=1	2.1074	0.1273	0.3888	3.9791	0.8101	2.5781
t=5	2.1081	0.1273	0.3888	3.9760	0.8090	2.5745
t=10	2.1082	0.1273	0.3887	3.9720	0.8077	2.5701
t=15	2.1077	0.1272	0.3886	3.9681	0.8063	2.5656
t=20	2.1060	0.1272	0.3886	3.9642	0.8050	2.5612

TABLE II

ERROR NORMS WITH DIFFERENT NUMBERS OF PARTICLES N AT $t=1$ FOR $dt=0.1$ AND $c=0.03,\ c=0.1$

N	$c=0.03$		$c=0.1$	
	L_2	L_∞	L_2	L_∞
101	1.5974×10^{-4}	4.6161×10^{-5}	2.9903×10^{-3}	7.9436×10^{-4}
201	4.1234×10^{-5}	1.2827×10^{-5}	5.6603×10^{-4}	2.4436×10^{-4}
401	1.2753×10^{-5}	4.4787×10^{-6}	2.3050×10^{-4}	1.0552×10^{-4}
801	7.5144×10^{-6}	2.4747×10^{-6}	1.8571×10^{-4}	7.2239×10^{-5}

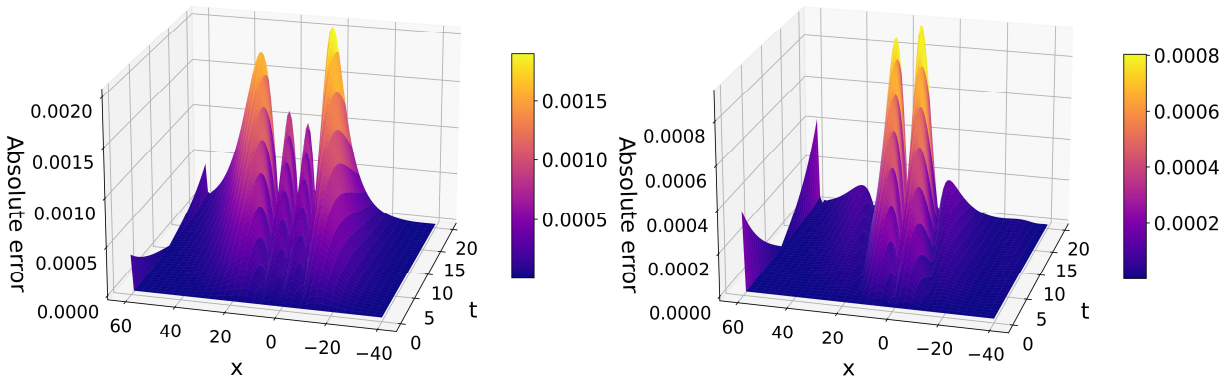

(a) Absolute error from SPH (b) Absolute error from KDF-SPH

Fig. 2. Space–time graph of absolute error through SPH and KDF-SPH at $dt=0.1$ and $N=101$ for $c=0.03$ from $t=0$ to $t=20$

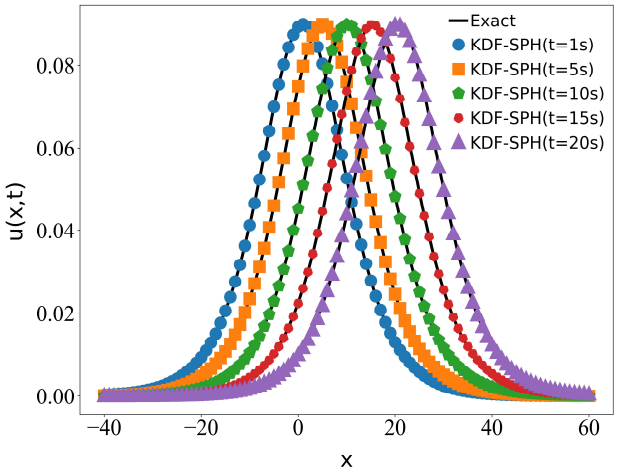

Fig. 3. A comparison graph of the exact solution and numerical solution

Case 2 Based on the conditions of the equation (3), the boundary condition is changed to $u(x_L,t)=u(x_R,t)=0$ for $t\in[0,T]$, while other conditions remain unchanged. The parameters are selected as $\alpha=2$, $\beta=1$, $x_0=0$, $c=1/6$, and the spatial domain $\Omega=[-50,50]$. TABLE III compares the L_2 norm errors of KDF-SPH with the numerical method from reference [29] at different time with $dx=0.05$ and $dt=0.1$. As shown in TABLE III, KDF-SPH achieves better results and higher accuracy than reference [29].

TABLE III
THE COMPARISON OF ERROR NORMS FOR CASE 2

time	*Chen*[29]	*KDF − SPH*
$t=0.2$	8.7931×10^{-4}	4.8966×10^{-4}
$t=0.4$	1.3187×10^{-3}	9.7979×10^{-4}
$t=0.6$	1.7480×10^{-3}	1.2251×10^{-3}
$t=0.8$	2.1970×10^{-3}	1.9618×10^{-3}
$t=1.0$	2.6359×10^{-3}	2.2538×10^{-3}

Two solitary waves motion

The interaction of two solitary waves is studied. The initial condition satisfies the following equation [30]

$$u(x,0)=\sum_{l=1}^{2}G_l sech^2[k_l(x-x_l)], \tag{32}$$

Where $G_l=3c_l$, $k_l=\frac{1}{2}\sqrt{\frac{c_l}{1+c_l}}$ and $v_l=1+c_l$.

For this example, the parameters are chosen as $\alpha=1$, $\beta=1$, $c_1=1/2$, $c_2=3/2$, $x_1=-10$, $x_2=-20$. The spatial domain $\Omega=[-50,50]$ for the numerical simulation , with the number of particles $N=501$, time step $dt=0.01$, and simulation time from $t=0$ s to $t=20$ s. For $l=1$ and 2, two solitary waves are labeled as wave A and wave B. Based on the above chosen parameters, The amplitude of wave A is $G_1=3/2$, and its wave speed is $v_1=3/2$. The amplitude of wave B is $G_2=9/2$, and its wave speed is $v_2=5/2$. This enables the accurate identification of the positions of the two waves in the numerical simulation graph. Figure 4 illustrates the evolution of the collision and interaction between wave A and wave B from $t=0s$ to $t=20s$. At $t=0s$, wave A is positioned ahead of wave B. Since the wave speed of wave B is greater than that of wave A, wave B gradually catches up to wave A over time until the two waves collide and merge into a single wave. As time progresses, wave B surpasses wave A (as seen at $t=6.5s$), and both waves eventually continue propagating forward. Additionally, the graph shows that after the collision of wave A and B, some of the three invariants experience a certain degree of loss. This numerical simulation case study can be effectively applied to model the interaction processes of oceanic solitary waves (such as tsunamis or internal solitary waves) and predict their amplitude variation patterns following collision and superposition. These findings provide important guidance for designing wave-resistant coastal and marine structures (like breakwaters and offshore platforms). They help prevent structural damage caused by dangerous wave actions, making these constructions safer and more durable.

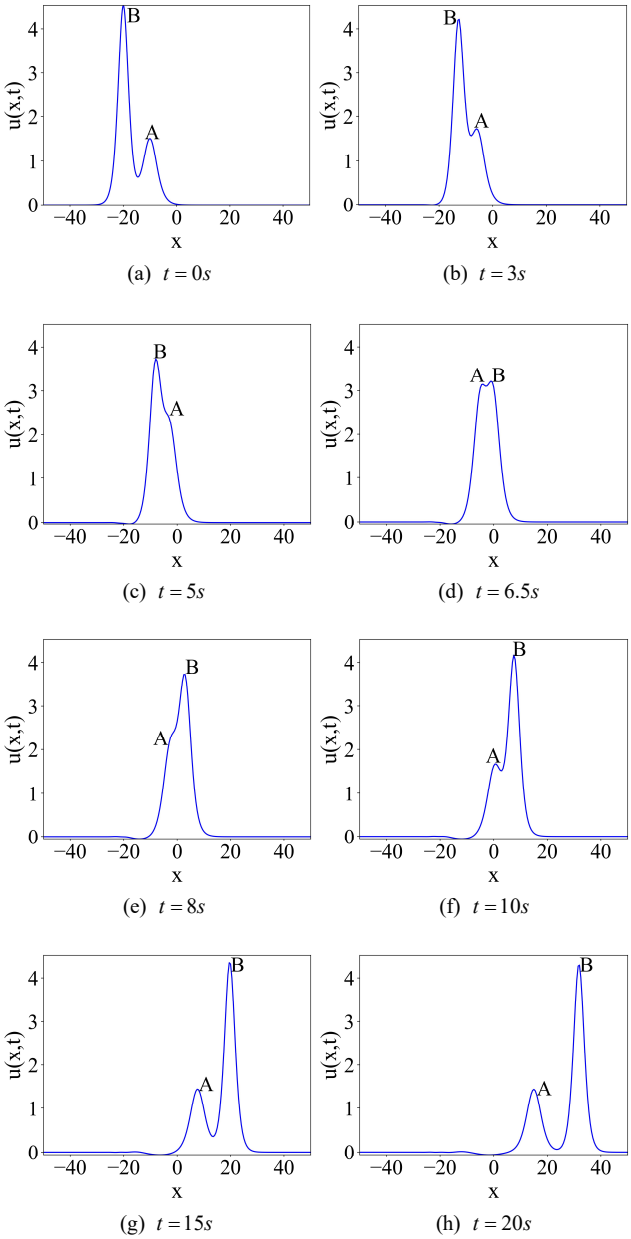

Fig. 4. The numerical simulation of the collision between two solitary waves

B. MRLW Equation

Single solitary wave motion

The exact solution of the MRLW equation (5) is given by [31] as follows

$$U(x,t)=\sqrt{c}\,sech[k(x-(c+1)t-x_0],\ (x,t)\in\Omega\times[0,T]. \quad (33)$$

where $k=\sqrt{\dfrac{c}{\beta(c+1)}}$.

For this problem, the computational forms of the above three invariants I_1, I_2, and I_3 are given by

$$I_1=\frac{\pi\sqrt{c}}{k}, I_2=\frac{2c}{k}+\frac{2\beta ck}{3}, I_3=\frac{4c^2}{3k}-\frac{2c\beta k}{3}. \quad (34)$$

Case 1 We take $c=0.05$, $x_0=40$ with the spatial domain $\Omega=[0,100]$. Based on Equation (34), the analytical values are calculated as $I_1=3.2192$, $I_2=0.4655$, $I_3=0.0080$. TABLE IV shows the invariants and error norms for the MRLW equation at different times with $c=0.05$, $dx=0.1$ and $dt=0.05$. The results are close to the analytical values and remain nearly constant. TABLE V presents the L_2 and L_∞ error norms for different particle numbers N at $t=5s$ using the SPH and the KDF-SPH. The proposed method yields smaller error norms compared to the SPH method, demonstrating its effectiveness for the MRLW equation. Figure 5 shows a 3D plot of the absolute error from $t=0$ s to $t=20$ s using the KDF-SPH with $N=101$ and $dt=0.05$. The maximum error occurs near the peak of the solitary wave. This observed phenomenon likely results from the extremely steep wave profile inducing near-infinite spatial gradients that dramatically amplify truncation errors in discrete numerical methods, combined with the complete breakdown of the dynamic dispersion-nonlinearity balance that normally maintains solitary wave stability in this critical region. Figure 6 presents a comparison plot between the analytical solution and the numerical solution of the equation for $N=1001$ and $dt=0.1$. The result shows good agreement between the two solutions.

Case 2 Based on the conditions of the equation (5), the boundary condition is changed to $u(x_L,t)=u(x_R,t)=0$, and the spatial domain $\Omega=[0,100]$. Other conditions remain unchanged. When $N=2001$ and $dt=0.001$, the result of this study is compared with the results from reference [32] for different time, as show in TABLE VI. This table presents the L_2 and L_∞ errors obtained by KDF-SPH and the method proposed in reference [32]. In reference [32], the selected number of particles is 2048. The method presented in this paper yields a smaller error result than that in Reference [32], even when a smaller number of particles is used. Through systematic numerical experiments and comprehensive analysis of the results, we can conclusively demonstrate that the KDF-SPH method proposed in this study exhibits significantly better simulation performance compared to the method proposed in reference [32].

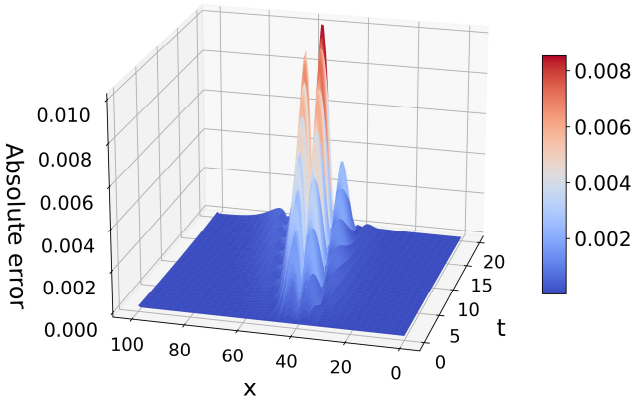

Fig. 5. The absolute error from $t=0s$ to $t=20s$

TABLE IV

VALUES OF THE CONSERVED QUANTITIES, L_2 ERROR AND L_∞ ERROR WITH $dx=0.1$, $dt=0.05$ AND $c=0.05$ AT VARIOUS TIME LEVELS

time	I_1	I_2	I_3	L_2	L_∞
$t=1$	3.2186	0.4654	0.0080	7.6050×10^{-5}	3.2102×10^{-4}
$t=5$	3.2175	0.4651	0.0080	3.8414×10^{-4}	1.6299×10^{-4}
$t=10$	3.2161	0.4646	0.0080	7.7691×10^{-4}	3.3145×10^{-4}
$t=15$	3.2145	0.4642	0.0079	1.1812×10^{-3}	5.0704×10^{-4}
$t=20$	3.2127	0.4637	0.0079	0.6019×10^{-3}	6.9081×10^{-4}

TABLE V

ERROR NORMS WITH $c=0.05$, $t=5$ AND $dt=0.1$ FOR DIFFERENT NUMBERS OF PARTICLES N

N	*SPH*		*KDF − SPH*	
	L_2	L_∞	L_2	L_∞
101	1.9745×10^{-3}	7.6143×10^{-3}	7.4997×10^{-3}	2.8332×10^{-3}
201	1.5063×10^{-2}	5.6630×10^{-3}	2.0867×10^{-3}	9.3461×10^{-4}
401	1.3949×10^{-2}	5.1648×10^{-3}	9.2126×10^{-4}	4.4321×10^{-4}
801	1.3677×10^{-2}	5.0396×10^{-3}	7.6324×10^{-4}	3.2001×10^{-4}

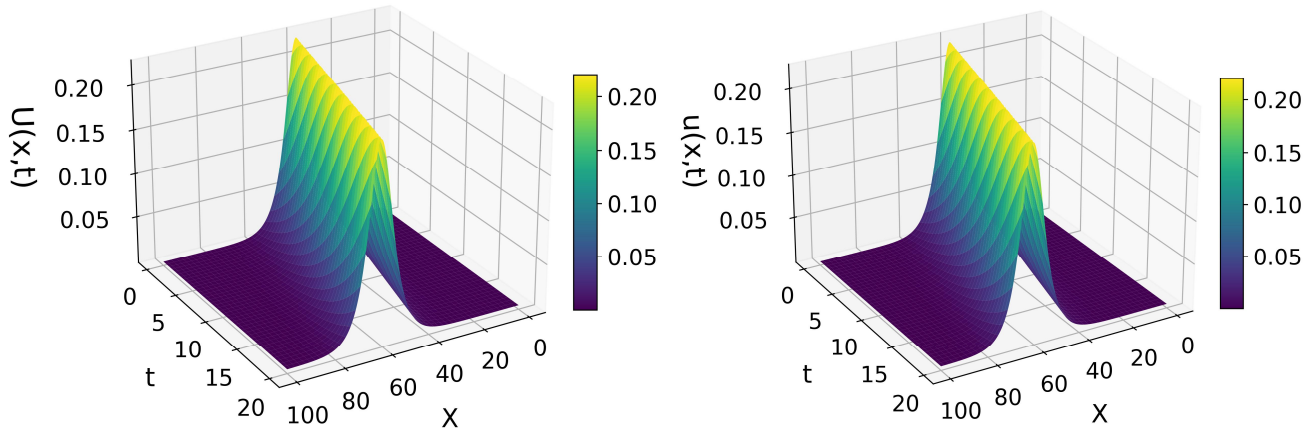

(a) Space–time graph of the exact solution (b) Space–time graph of the numerical solution

Fig. 6. Space–time graph of the exact solution and the numerical solution at $dt = 0.1$ and N=1001 from $t = 0$ s to $t = 20$ s

TABLE VI
THE COMPARISON OF ERROR NORMS FOR CASE 2

time	*HanyN.Hassan*[32]		*KDF – SPH*	
	L_2	L_∞	L_2	L_∞
$t = 2$	1.67083×10^{-4}	4.67942×10^{-5}	3.03585×10^{-5}	1.22263×10^{-5}
$t = 4$	2.44839×10^{-4}	6.84808×10^{-5}	6.07609×10^{-5}	2.38171×10^{-5}
$t = 6$	2.33647×10^{-4}	6.51000×10^{-5}	9.10839×10^{-5}	3.47722×10^{-5}
$t = 8$	3.11637×10^{-4}	8.71898×10^{-5}	1.21226×10^{-4}	4.53936×10^{-5}
$t = 10$	4.78729×10^{-4}	1.34767×10^{-4}	1.51112×10^{-4}	5.66905×10^{-5}

Two solitary waves motion

In this part, we study the collision of two solitary waves. The initial condition is given by [12]

$$u(x,0) = \sum_{m=1}^{2} \sqrt{c_m}\, sech[k_m (x - x_m)], \tag{35}$$

where $k_m = \sqrt{\dfrac{c_m}{1+c_m}}$.

Reference [12] provides the specific analytical values of the three invariants related to this problem.

$$\begin{aligned} I_1 &= \sum_{m=1}^{2} \frac{\pi\sqrt{c_m}}{k_m}, \\ I_2 &= \sum_{m=1}^{2} \left(\frac{2c_m}{k_m} + \frac{2\beta c_m k_m}{3} \right), \\ I_3 &= \sum_{m=1}^{2} \left(\frac{4c_m^2}{3k_m} - \frac{2\beta c_m k_m}{3} \right). \end{aligned} \tag{36}$$

We take $c_1 = 0.2$, $c_2 = 0.1$, $x_1 = 15$ and $x_2 = 35$. The domain spans $\Omega = [0,100]$, discretized by 501 particles. The simulation time ranges from $t = 0$ s to $t = 20$ s with $dt = 0.1$. The analytical values of the three invariants are calculated as $I_1 = 6.7364$, $I_2 = 1.7177$, $I_3 = 0.1003$. TABLE VII presents the simulated values of the three invariants I_1, I_2, and I_3. Comparison with the analytical values shows that the relative motion between two waves leads to a loss in the three invariants. Figure 7 displays the detailed simulation results of the interaction between two solitary waves at different time. The wave peak amplitude exhibits minor attenuation, indicating that wave interactions cause slight energy dissipation. For practical applications, controlling solitary wave interactions optimize breakwater energy dissipation in shallow waters.

TABLE VII
VALUES OF THE CONSERVED QUANTITIES AT DIFFERENT TIME

time	I_1	I_2	I_3
$t = 0$	6.7317	1.7386	0.1051
$t = 4$	6.6906	1.7100	0.0998
$t = 8$	6.6505	1.6832	0.0950
$t = 12$	6.6133	1.6582	0.0906
$t = 16$	6.5785	1.6351	0.0867
$t = 20$	6.5460	1.6136	0.0833

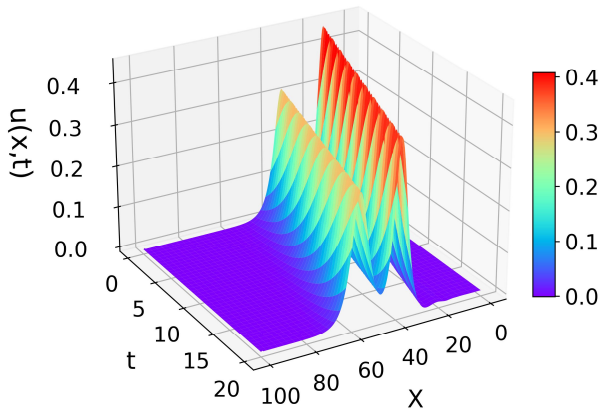

Fig. 7. Simulation graph of the interaction between two solitary waves from $t = 0$ s to $t = 20$ s

C. GRLW Equation

The exact solution of the GRLW equation (7) is given by [33] as follows

$$U(x,t)=[A\mathrm{sech}^2\left(k(x-vt-x_0)\right)]^{\frac{1}{p}}, \tag{37}$$

where $A=\dfrac{c(p+1)(p+2)}{2}$, $v=1+\alpha c$, $k=\dfrac{p}{2\sqrt{\beta}}\sqrt{\dfrac{\alpha c}{v}}$.

We take $\alpha=1$, $\beta=1$, $c=0.03$, $x_0=40$ and choose the spatial domain $\Omega=[0,100]$. When $p=3,4,5$ in equation (7), TABLE VIII presents the L_2 and L_∞ error norms computed using the SPH and KDF-SPH methods with $N=101$ at $t=0.1$ s, $t=0.5$ s and $t=1$ s. For $p=3,4,5$ in equation (7), TABLE IX shows the L_2 and L_∞ error norms. These norms are calculated using both SPH and KDF-SPH with different numbers of particles and a time step $dt=0.1$ at $t=1$ s. The numerical results in these two tables indicate that KDF-SPH yields smaller error norms than the traditional SPH, which confirms its accuracy. Concurrently, these experimental results substantiate that the improved SPH method enhances both numerical accuracy and simulation efficacy to a certain extent.

VII. Conclusion and Future Perspectives

Based on the study of using SPH to solve nonlinear partial differential equations, we find that its accuracy is relatively low. Therefore, this paper proposes a meshless method based on the KDF-SPH approximation. Firstly, the GRLW equation is discretized to derive a discrete numerical scheme and unconditional stability is confirmed by plotting the eigen values of the matrix of iterations. Then, KDF-SPH is applied to simulate single solitary wave propagation, the collision of double solitary waves, and the development of wave patterns, thereby validating its effectiveness. Both the L_2 error norm and L_∞ error norm demonstrate that KDF-SPH achieves high accuracy. Moreover, the calculation of the three conservation invariants for the test problem demonstrates that the proposed method exhibits good conservation properties for the GRLW equation. Under identical numerical conditions, the results obtained by KDF-SPH in this study show higher numerical accuracy compared to both traditional SPH and existing methods reported in the literature. These comparisons confirm the proposed method achieves higher numerical accuracy and shows better suitability for solving the GRLW equation. In conclusion, the proposed meshless method exhibits good performance as a numerical solver for the GRLW equation, showing the practical applicability and the computational effectiveness. And KDF-SPH exhibits better advantages over the traditional SPH.

Building upon the excellent performance of the KDF-SPH method in solving the GRLW equation, future research can be expanded in multiple dimensions. The method can be extended to two-dimensional or higher-dimensional GRLW equation to simulate more complex wave phenomena in practical engineering applications. Additionally, its applicability could be further explored for a broader range of nonlinear PDEs. Regarding the phenomenon observed in this study where the maximum absolute error in solitary wave simulations predominantly occurs near the wave peak, subsequent research should conduct more in-depth theoretical investigations and develop targeted solutions. Theoretically, emphasis should be placed on establishing rigorous convergence criteria and error bounds under strongly nonlinear conditions to further refine the theoretical framework. Future work should particularly focus on examining the capability of this method in handling wave-breaking phenomena and its coupling mechanisms with structural response models, which are of critical importance for offshore engineering applications. The proposed development directions maintain the meshless advantages while potentially overcoming current limitations in computational scale and physical fidelity for industrial-scale problems. In summary, this method holds boundless potential for diverse applications.

TABLE VIII
Comparison of error norms at different times for different methods

p	*Methods*	*Error norm*	t=0.1	t=0.5	t=1
$p=3$	*SPH*	L_2	1.0486×10^{-3}	5.2425×10^{-3}	1.0479×10^{-2}
		L_∞	4.0108×10^{-4}	2.0360×10^{-3}	3.9227×10^{-3}
	KDF – SPH	L_2	3.8985×10^{-4}	1.9503×10^{-3}	3.9026×10^{-3}
		L_∞	1.6359×10^{-4}	8.0954×10^{-4}	1.6005×10^{-3}
$p=4$	*SPH*	L_2	1.7197×10^{-3}	8.5981×10^{-3}	1.7182×10^{-2}
		L_∞	7.3676×10^{-4}	3.5858×10^{-3}	7.2875×10^{-3}
	KDF – SPH	L_2	6.3404×10^{-4}	3.1746×10^{-3}	6.3583×10^{-3}
		L_∞	2.8338×10^{-4}	1.4688×10^{-4}	2.8836×10^{-3}
$p=5$	*SPH*	L_2	2.3498×10^{-3}	1.1759×10^{-2}	2.3482×10^{-2}
		L_∞	1.1007×10^{-3}	5.2464×10^{-3}	1.0595×10^{-2}
	KDF – SPH	L_2	8.7696×10^{-4}	4.3972×10^{-3}	8.8222×10^{-3}
		L_∞	4.4063×10^{-4}	2.1438×10^{-3}	4.4305×10^{-3}

TABLE Ix
COMPARISON OF ERROR NORMS WITH DIFFERENT NUMBERS OF PARTICLES FOR DIFFERENT METHODS

p	*Methods*	*Error norm*	$N=101$	$N=201$	$N=401$	$N=801$
$p=3$	*SPH*	L_2	1.0479×10^{-2}	8.0631×10^{-3}	7.4965×10^{-3}	7.3583×10^{-3}
		L_∞	3.9227×10^{-3}	3.0219×10^{-3}	2.8098×10^{-3}	2.7494×10^{-3}
	KDF – SPH	L_2	3.9026×10^{-3}	1.0774×10^{-3}	4.8946×10^{-4}	4.1911×10^{-4}
		L_∞	1.6006×10^{-3}	5.2259×10^{-4}	2.4792×10^{-4}	1.7893×10^{-4}
$p=4$	*SPH*	L_2	1.7182×10^{-2}	1.3324×10^{-2}	1.2401×10^{-2}	1.2174×10^{-2}
		L_∞	7.2875×10^{-3}	5.6849×10^{-3}	5.2924×10^{-3}	5.2090×10^{-3}
	KDF – SPH	L_2	6.3583×10^{-3}	1.8589×10^{-3}	1.0037×10^{-3}	9.1329×10^{-4}
		L_∞	2.8836×10^{-3}	1.0172×10^{-3}	5.3639×10^{-4}	4.1421×10^{-4}
$p=5$	*SPH*	L_2	2.3482×10^{-2}	1.8338×10^{-2}	1.7100×10^{-2}	1.6796×10^{-2}
		L_∞	1.0595×10^{-2}	8.4538×10^{-3}	7.9485×10^{-3}	7.8385×10^{-3}
	KDF – SPH	L_2	8.8222×10^{-3}	2.7665×10^{-3}	1.7135×10^{-3}	1.6100×10^{-3}
		L_∞	4.4305×10^{-3}	1.6570×10^{-3}	9.4592×10^{-4}	7.7091×10^{-4}

REFERENCES

[1] Sungnul S, Para K, Moore E J, et al. "A Finite Difference Method for Solution of Integer-order and Caputo Fractional-time Advection-Diffusion-Reaction Equations: Convergence Analysis and Application to Air Pollution," Engineering Letters, vol. 33, no. 2, pp. 292-311, 2025.

[2] D. H. Peregrine, "Long waves on a beach," Journal of Fluid Mechanics, vol. 27, no. 4, pp. 815-827, 1967.

[3] S. Kutluay and A. Esen, "A finite difference solution of the regularized long-wave equation," Mathematical Problems in Engineering, vol. 2006, no. 1, pp. 085743, 2006.

[4] J. Sun, N. Tao, T. Zhang, P. Yan, "Numerical solution of the RLW equation using the cosine differential quadrature method," Journal of Northwest Normal University (Natural Science Edition), vol. 47, no. 5, pp. 30-34, 39, 2011.

[5] M. Z. Görgülü, I. Dag, and D. Irk, "Simulations of solitary waves of RLW equation by exponential B-spline Galerkin method," Chinese Physics B, vol. 26, no. 8, pp. 180–202, 2017.

[6] X. Yang, L. Zhang, and Y. Ge, "High-order compact finite difference schemes for solving the regularized long-wave equation," Applied Numerical Mathematics, vol. 185, pp. 165-187, 2023.

[7] K. R. Raslan, "Numerical study of the modified regularized long wave (MRLW) equation," Chaos, Solitons \& Fractals, vol. 42, no. 3, pp. 1845-1853, 2009.

[8] J. Cai, "A multisymplectic explicit scheme for the modified regularized long-wave equation," Journal of Computational and Applied Mathematics, vol. 234, no. 3, pp. 899-905, 2010.

[9] Y. Gao and L. Mei, "Mixed Galerkin finite element methods for modified regularized long wave equation," Applied Mathematics and Computation, vol. 258, pp. 267-281, 2015.

[10] S. R. Jena, A. Senapati, and G. S. Gebremedhin, "Approximate solution of MRLW equation in B-spline environment," Mathematical Sciences, vol. 14, no. 4, pp. 345-357, 2020.

[11] Y. Xu, J. Hu, and C. Hu, "A new conservative difference scheme for the generalized regularized long wave equation," Journal of Sichuan University (Natural Science Edition), vol. 48, no. 3, pp. 534-538, 2011.

[12] D. A. Hammad and M. S. El-Azab, "Chebyshev–Chebyshev spectral collocation method for solving the generalized regularized long wave (GRLW) equation," Applied Mathematics and Computation, vol. 285, pp. 228-240, 2016.

[13] H. Zheng, Y. Xia, Y. Bai, et al., "Travelling wave solutions of the general regularized long wave equation," Qualitative Theory of Dynamical Systems, vol. 20, no. 1, pp. 8, 2021.

[14] A. Kumari and V. K. Kukreja, "Study of generalized regularized long wave equation via septic Hermite collocation method with Crank–Nicolson and SSP-RK43 schemes to capture the various solitons," Wave Motion, vol. 122, pp. 103188, 2023.

[15] J. J. Monaghan, "Smoothed particle hydrodynamics," Annual Review of Astronomy and Astrophysics, vol. 30, pp. 543-574, 1992.

[16] L. B. Lucy, "A numerical approach to the testing of the fission hypothesis," Astronomical Journal, vol. 82, pp. 1013-1024, 1977.

[17] J. K. Chen, J. E. Beraun, and C. J. Jih, "An improvement for tensile instability in smoothed particle hydrodynamics," Computational Mechanics, vol. 23, pp. 279-287, 1999.

[18] J. Chen, F. Xu, and Q. Huang, "Research on smoothed particle hydrodynamics method," Journal of Mechanical Strength, vol. 30, no. 1, pp. 78-82, 2008.

[19] J. Cai, "Multisymplectic numerical method for the regularized long-wave equation," Computer Physics Communications, vol. 180, no. 10, pp. 1821-1831, 2009.

[20] Y. Gao and L. Mei, "Mixed Galerkin finite element methods for modified regularized long wave equation," Applied Mathematics and Computation, vol. 258, pp. 267-281, 2015.

[21] S. R. Jena, A. Senapati, and G. S. Gebremedhin, "Approximate solution of MRLW equation in B-spline environment," Mathematical Sciences, vol. 14, no. 4, pp. 345-357, 2020.

[22] F. Chen and G. Wei, "A review of smoothed particle hydrodynamics family methods for multiphase flow," Chinese Journal of Theoretical and Applied Mechanics, vol. 53, no. 9, pp. 2357-2373, 2021.

[23] D. Feng and R. Imin, "A kernel derivative free SPH method," Results in Applied Mathematics, vol. 17, pp. 100355, 2023.

[24] A. Bashan and N. M. Yağmurlu, "A mixed method approach to the solitary wave, undular bore and boundary-forced solutions of the Regularized Long Wave equation," Computational and Applied Mathematics, vol. 41, no. 4, pp. 169, 2022.

[25] A. Ali and S. Haq, "A computational modeling of the behavior of the two-dimensional reaction–diffusion Brusselator system," Applied Mathematical Modelling, vol. 34, no. 12, pp. 3896-3909, 2010.

[26] M. B. Liu and G. R. Liu, "Smoothed Particle Hydrodynamics," Archives of Computational Methods in Engineering, vol. 17, no. 1, pp. 25-76, 2010.

[27] S. Haq and A. Ali, "A meshfree method for the numerical solution of the RLW equation," Journal of Computational and Applied Mathematics, vol. 223, no. 2, pp. 997-1012, 2009.

[28] S. I. Zaki, "Solitary waves of the splitted RLW equation," Computer Physics Communications, vol. 138, no. 1, pp. 80-91, 2001.

[29] J. Chen and X. Shao, "A novel conservative difference method for solving the generalized regularized long wave equation," Journal of Shenyang University (Natural Science Edition), vol. 30, no. 2, pp. 163-172, 2018.

[30] B. Wang, T. Sun, and D. Liang, "The conservative and fourth-order compact finite difference schemes for regularized long wave equation," Journal of Computational and Applied Mathematics, vol. 356, pp. 98-117, 2019.

[31] S. R. Jena, A. Senapati, and G. S. Gebremedhin, "Approximate solution of MRLW equation in B-spline environment," Mathematical Sciences, vol. 14, no. 4, pp. 345-357, 2020.

[32] H. N. Hassan, "An efficient numerical method for the modified regularized long wave equation using Fourier spectral method," Journal of the Association of Arab Universities for Basic and Applied Sciences, vol. 24, pp. 198-205, 2017.

[33] R. Mohammadi, "Exponential B-spline collocation method for numerical solution of the generalized regularized long wave equation," Chinese Physics B, vol. 24, no. 5, pp. 050206, 2015.